

Mongolian Mountains Matter Most: Impacts of the Latitude and Height of Asian Orography on Pacific Wintertime Atmospheric Circulation

R. H. WHITE

Joint Institute for the Study of Atmosphere and Ocean, University of Washington, Seattle, Washington

D. S. BATTISTI

Department of Atmospheric Sciences, University of Washington, Seattle, Washington

G. H. ROE

Department of Earth and Space Sciences, University of Washington, Seattle, Washington

(Manuscript received 21 May 2016, in final form 12 January 2017)

ABSTRACT


The impacts of Asian orography on the wintertime atmospheric circulation over the Pacific are explored using altered-orography, semi-idealized, general circulation model experiments. The latitude of orography is found to be far more important than height. The Mongolian Plateau and nearby mountain ranges, centered at $\sim 48^{\circ}\text{N}$, have an impact on the upper-level wintertime jet stream that is approximately 4 times greater than that of the larger and taller Tibetan Plateau and Himalayas to the south. Key contributing factors to the importance of the Mongolian mountains are latitudinal variations in the meridional potential vorticity gradient and the strength of the impinging wind—both of which determine the amplitude of the atmospheric response—and the structure of the atmosphere, which influences the spatial pattern of the downstream response. Interestingly, while the Mongolian mountains produce a larger response than the Tibetan Plateau in Northern Hemisphere winter, in April–June the response from the Tibetan Plateau predominates. This result holds in two different general circulation models. In experiments with idealized orography, varying the plateau latitude by 20° , from 43° to 63°N , changes the response amplitude by a factor of 2, with a maximum response for orography between 48° and 53°N , comparable to the Mongolian mountains. In these idealized experiments, the latitude of the maximum wintertime jet increase changes by only $\sim 6^{\circ}$. It is proposed that this nearly invariant spatial response pattern is due to variations in the stationary wavenumber with latitude leading to differences in the zonal versus meridional wave propagation.

1. Introduction

Earth's major mountain belts and plateaus have a significant impact on its climate (Charney and Eliassen 1949). In northern midlatitudes, orography plays a large role in setting zonal asymmetries in continental temperature and precipitation (e.g., Seager et al. 2002), sharpening the eddy-driven zonal jet, and strengthening the storm tracks (e.g., Inatsu et al. 2002; Brayshaw et al. 2009). In the

tropics, the Andes play a role in the off-equatorial displacement of the climatological intertropical convergence zone (ITCZ) in the eastern Pacific, which is fundamental to the El Niño–Southern Oscillation (Takahashi and Battisti 2007; Maroon et al. 2015). In summer, the mechanical effect of orography plays a critical role in setting the intensity of monsoonal precipitation throughout the subtropics (e.g., Boos and Kuang 2010; Molnar et al. 2010). It has even been suggested that the North American Cordillera may have a sufficiently large impact on atmospheric circulation to influence oceanic meridional overturning circulation (e.g., Warren 1983).

In midlatitudes, the dominant mechanism through which orography has a large-scale climatic impact is the forcing of stationary Rossby waves. After the pioneering work of Charney and Eliassen (1949) and Smagorinsky

 Denotes content that is immediately available upon publication as open access.

Corresponding author e-mail: R. H. White, rachel.white@cantab.net

(1953), there was a resurgence of research on the impact of orography on stationary waves in the 1980s and 1990s, beginning with Hoskins and Karoly (1981). Much of this work was performed with dedicated numerical stationary wave models, in which the orographic perturbation is applied as a lower boundary condition and the steady-state response found. Such models solve linear or nonlinear versions of the primitive or quasigeostrophic equations for a prescribed background zonal-mean flow (e.g., Hoskins and Karoly 1981; Nigam and Lindzen 1989; Held and Ting 1990; Hoskins and Ambrizzi 1993; Ringler and Cook 1999). Atmospheric general circulation models (AGCMs) have also been used to study idealized orography in aquaplanet simulations (e.g., Nigam et al. 1988; Cook and Held 1992; Ringler and Cook 1995), as well as real-world orography in configurations with present-day landmasses (e.g., Manabe and Terpstra 1974; Hahn and Manabe 1975; Broccoli and Manabe 1992; Held et al. 2002). Orographically forced Rossby waves impact the energy exchange between the atmosphere and ocean, thereby further affecting the atmospheric circulation and impacting the buoyancy driving of the ocean (e.g., Kitoh 2004).

More recent studies by Brayshaw et al. (2009) and Saulière et al. (2012) have drawn on the results from linear stationary wave modeling studies to help interpret results from a series of experiments using complex GCMs. These experiments illuminated how the North American Cordillera increase the strength of the downstream Atlantic jet stream and storm track and increase the southwest–northeast tilt of the jet.

The majority of realistic-orography studies remove all orography globally and attribute the response over North America and the Atlantic to the North American Cordillera (commonly referred to as the Rockies) and that over Asia and across the Pacific to the Tibetan Plateau (e.g., Manabe and Terpstra 1974; Hahn and Manabe 1975; Broccoli and Manabe 1992; Ringler and Cook 1999; Held et al. 2002; Kitoh 2002; Wilson et al. 2009; Saulière et al. 2012). However, a recent modeling study by Shi et al. (2015) found that, despite its lesser extent and elevation, the Mongolian Plateau may have a greater impact on the Pacific jet stream than the Tibetan Plateau. Here we explore this surprising result in depth, performing detailed analysis of the simulated responses to both realistic and idealized Asian orography and furthering our understanding of the underlying mechanisms.

We present a study of the impacts of orography of various heights and locations in Asia on the wintertime atmospheric circulation over the Pacific. We use the real-world land–sea distribution and flatten parts of the realistic orography, first analyzing the response to all central and East Asian orography (section 3) and then

isolating the impact of the Mongolian Plateau from that of the Tibetan Plateau (section 4). Using idealized orography, we consider the impact of orographic latitude (section 5b) and height (section 5c). In section 6, we discuss how our results compare to those expected from stationary wave theory.

Theoretical orographic impacts

Consider air impinging on orography in the presence of meridional temperature gradients. The air has two possible routes: it can flow up and over the orography (vertical deflection, often referred to as uplift), or be blocked and flow around it (horizontal deflection). We discuss each of these scenarios in turn.

With vertical deflection, adiabatic cooling associated with the forced upward motion on the windward flank of the mountain is balanced by horizontal advection of warm air by an induced poleward flow (Hoskins and Karoly 1981). The converse is true for the downward flow on the lee side, resulting in an induced equatorward flow. For westerly background flow (representative of midlatitudes), these motions combine to give anticyclonic circulation over the mountain. By the conservation of potential vorticity (PV), a cyclonic anomaly is produced downstream of the mountain. Advection of planetary vorticity by the resulting meridional flow results in an upwind shift of these circulation anomalies (Valdes and Hoskins 1991), resulting in a low-level anomalous streamfunction pattern similar to that depicted in Fig. 1a. The magnitude of the vorticity forcing is proportional to $(f/H)\mathbf{u} \cdot \nabla h$, where f is the Coriolis parameter, H is the scale height of the atmosphere, \mathbf{u} is a representative wind vector impinging on the mountain, h is the height of the mountain, and ∇ is the horizontal gradient operator (see, e.g., Held 1983). The value of $\mathbf{u} \cdot \nabla h$ has typically been approximated by the zonal component, $U(\partial h/\partial x)$, at a height between 1000 and 850 mb (Valdes and Hoskins 1991).

Horizontal deflection of zonal flow results in northward flow to the north and upwind of the orography and/or southward flow to the south. By the conservation of PV, this results in anticyclonic circulation to the north of the mountain and/or cyclonic circulation to the south (Valdes and Hoskins 1991) (see Fig. 1b). The magnitude of the PV forcing away from the lower boundary is given by $q' = -q_y\eta$, where q is the background PV, the subscript y denotes the meridional gradient $\partial/\partial y$, and η is the northward displacement of a fluid parcel, which can be approximated as half the meridional extent of the mountain (Valdes and Hoskins 1991).

Hereafter, we refer to responses with a west–east dipole of low-level (850 mb) anticyclonic and cyclonic circulation anomalies centered at the mountain latitude

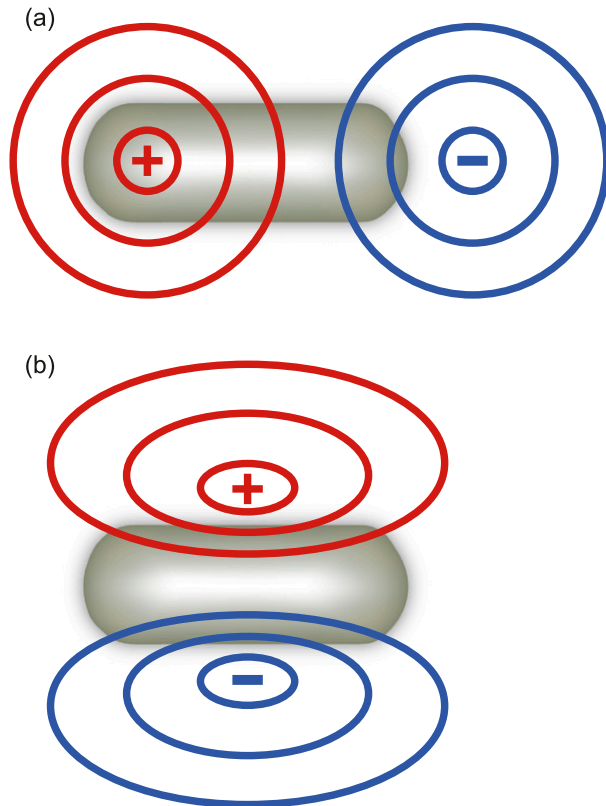


FIG. 1. Schematic depicting: (a) a vertical-deflection response and (b) a horizontal-deflection response to a Gaussian mountain plateau represented by gray shading. Red (blue) lines show lines of positive (negative) streamfunction anomaly ψ' . In (a), the anomalies are shifted upwind (relative to the baroclinic result of an anticyclone centered on the mountain) to represent the effects of advection.

(Fig. 1a) as vertical-deflection responses. Responses featuring a low-level north–south-orientated dipole of circulation anomalies (Fig. 1b) are referred to as horizontal-deflection responses.

Whether orography produces horizontal or vertical deflection, or a combination of the two, depends on the background temperature gradients, atmospheric stratification, and the shape and size of the orography (Valdes and Hoskins 1991; Brayshaw et al. 2009). One common assumption is that impinging air will follow the path along which it experiences the smallest perturbation in potential temperature θ : if the variation in θ following a path over the top of the orography is greater than that for a path traveling horizontally around the orography (i.e., $\theta_z h > |\theta_y \eta|$), then horizontal deflection will dominate (Valdes and Hoskins 1991). Horizontal deflection is therefore more likely for higher mountains or those that are less meridionally extensive.

Historically, in most linear stationary wave models, the deflected circulation $\Delta \mathbf{u}$ could not interact with the imposed orography, with the result that a vertical-deflection

response was predetermined by these models (Valdes and Hoskins 1991). In the literature, vertical deflection is often referred to as “linear forcing,” relative to the “nonlinear forcing” of horizontal deflection. We avoid this use of linear and nonlinear for the forcing terms to avoid ambiguity with nonlinearities within the interior of the flow.

2. Experimental setup and analysis methods

The experiments in this study are performed with the Community Atmosphere Model (CAM4) within the Community Earth System Model, version 1.0.5, (CESM1) architecture (Hurrell et al. 2013), with a horizontal resolution of $\sim 1.9^\circ \times 2.5^\circ$ and 26 vertical levels. The standard CESM orographic data are used: USGS global orography smoothed to the resolution of the model. Most experiments are performed with monthly mean climatological sea surface temperatures (SSTs) and sea ice from the merged Hadley–NOAA Optimum Interpolation (NOAA/OI) dataset (Hurrell et al. 2008). We also perform a limited set of secondary experiments using the CAM4 coupled to a slab ocean within the CESM framework. Cyclostationary slab-ocean q fluxes are imposed to ensure the control climate SSTs match observations. In these secondary experiments, the surface heat fluxes and SST can adjust self-consistently when the orographic perturbations are imposed.

Our primary control experiment (CTL) retains all of the world’s present-day orography. In our first set of experiments, we flatten specific regions of the present-day orography to a height of 50 m above mean sea level, similar to the elevation of the surrounding plains. The effect of the orography in question is found relative to the CTL simulation. For efficiency of description, we group together all orography between approximately 38.0° to 60.0°N and 65.0° to 152.5°E , encompassing the Mongolian Plateau and the Altai, Hangayn, Tien Shan, Sayan, Baykai, and Hentiyn Mountain Ranges as the “Mongolian Plateau.” Similarly, we collectively refer to all orography between approximately 10° to 42°N and 62° to 125°E , encompassing the Tibetan and Yunnan Plateaus, and the Greater Himalaya, Hindu Kush, Indo-Burma, Karakoram, Kunlun Shan, Pamirs, and associated mountain ranges; we refer to this combined orography as the “Tibetan Plateau.” Figure 2 shows the relevant orography, with these regions shown by dashed (Mongolian Plateau) and solid (Tibetan Plateau) outlines. Some overlap between these regions occurs due to the smoothing applied at the boundaries to avoid creating artificially steep orographic walls. Gaussian smoothing is applied in a 6-gridbox-wide “sponge” region at each boundary. Within the sponge region, the height is given by $h = \max[50.0, f(x, y)h_0]$, where max is

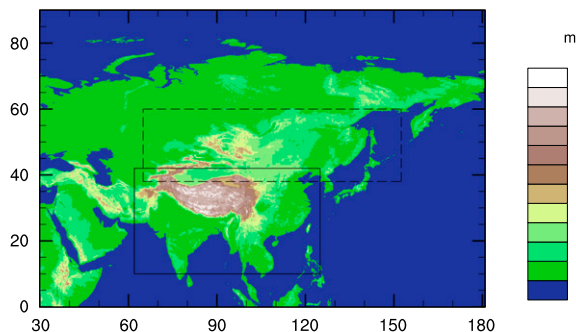


FIG. 2. Orographic map of the study region. The solid black box shows orography flattened for Tibetan Plateau experiments; the dashed box shows orography flattened for Mongolian Plateau experiments.

the maximum function, $f(x, y)$ is a Gaussian function of magnitude 1.0 at the outermost grid box to 0.0 at the innermost grid box, and h_0 is the topographic height from the USGS dataset.

In section 5, we also perform idealized plateau experiments, in which all global topography is flattened to 50 m above sea level, and then a Gaussian-edged plateau with a flat top is added. The effect of the orography is found relative to a flat control experiment (flat-CTL) with all land at 50 m above mean sea level. Flattening all orography alters the background atmospheric circulation into which the idealized plateaus are placed; this will contribute to some differences from the realistic-orography experiments (Held and Ting 1990).

The CESM requires the specification of the standard deviation of subgrid-scale orography S_d for the parameterization of the effects of subgrid-scale orography, including on gravity wave drag (following McFarlane 1987). In the flattened orography regions, we specify S_d to be equal to the S_d values from the CTL dataset for a flat region of Asia ($\sim 54^\circ\text{N}$, 42.5°E). For the sponge regions and idealized orography, we vary S_d linearly with height, with maximum values representative of high Asian orography ($\sim 30^\circ\text{N}$, 80°E).

Simulations are run for either 41 years (realistic-orography and slab-ocean experiments) or 31 years (idealized orography), with the first year discarded as a spinup period (11 years for the slab-ocean experiments). The Northern Hemisphere jet streams and storm tracks are strongest during winter (DJF); as such, we focus on DJF means. Figures present the differences from a control simulation such that they show the impact of the orography in question. Hence, for realistic-orography simulations, we plot CTL minus experiment; for idealized orography simulations, we plot experiment minus flat-CTL.

The impact of orography on circulation is characterized by the eddy streamfunction ψ' ; ψ' is the departure

of the streamfunction ψ from the zonal mean $[\psi]$. We examine both low-level (850 mb) and upper-level (250 mb) ψ' , as well as low-level θ and upper-level zonal wind U .

Within the midlatitudes, patterns of climatological mean ψ' can indicate the forcing of stationary Rossby waves. The meridional and vertical propagation of zonal-mean stationary wave activity within a zonal-mean flow can be illustrated by the Eliassen–Palm fluxes (EP fluxes; Eliassen and Palm 1961; Andrews and McIntyre 1976; Edmon et al. 1980). We follow the scaling of the quasigeostrophic EP flux vectors and divergence of Edmon et al. (1980), omitting the scaling of $2\pi a^2/g$ (a is Earth's radius).

EP flux theory has been extended to examine zonally varying stationary wave activity fluxes on a zonal-mean background flow (Plumb 1985) and, more recently, to also allow for a zonally varying background flow (Takaya–Nakamura fluxes; Takaya and Nakamura 1997, 2001). We use the Takaya–Nakamura stationary wave activity fluxes to examine the horizontal propagation of the stationary waves forced by orography. In our calculations, the perturbations in the wave activity flux are differences created by the orography: for example, CTL minus no Mongolia. The flux is mathematically constructed to be independent of the phase of the Rossby wave; the flux magnitude is therefore related to the phase-independent Rossby wave amplitude following the wave group velocity (Takaya and Nakamura 2001). Several assumptions are made to achieve this phase independence for a zonally varying flow, so we use the flux vectors only qualitatively to help interpret the patterns of ψ' created by orography.

To help understand the paths of the orography-forced stationary Rossby waves illuminated by the Takaya–Nakamura wave activity fluxes, we make use of the local Rossby stationary wavenumber $K_s = (\beta_*/U)^{1/2}$, where β_* is the meridional gradient of absolute vorticity. Following Hoskins and Ambrizzi (1993), we calculate the equivalent stationary zonal wavenumber K_s in the Mercator coordinate system. For stationary waves, $k^2 + l^2 = K_s^2$ (e.g., Hoskins and Karoly 1981), where k and l are the local zonal and meridional wavenumbers, respectively. Imagine a localized Rossby wave source producing waves of zonal wavenumber k ; in regions where $k < K_s$, the stationary wave must have real l and so will propagate meridionally away from the source; conversely, where $k > K_s$, the stationary wave must have imaginary l , and waves will be evanescent in the meridional direction and are thus likely to be meridionally confined (Held 1983). Ray theory also dictates that Rossby waves are refracted toward latitudes with higher K_s . Regions where K_s decreases to both the north and south (i.e., a meridional maximum) can therefore act

as a Rossby waveguide (e.g., Hoskins and Ambrizzi 1993; Manola et al. 2013). These theoretical arguments have been developed for waves in a zonal-mean, time-mean flow that varies slowly in the meridional direction. Application to a flow that varies zonally, temporally, and that has locally strong meridional gradients should be considered only as a qualitative guide to Rossby wave behavior (Hoskins and Ambrizzi 1993); Lutsko and Held (2016) suggest viewing a sharp maximum in K_s as an indication of the potential of the flow for waveguide trapping.

Analysis of the control simulation

We compare the DJF climatology from the CTL simulation to ECMWF interim reanalysis (ERA-Interim) data averaged over 1979–2015 (Dee et al. 2011). Figures 3a (3b) and 3g (3h) show ψ' at lower and upper levels from ERA-Interim (CTL). The model is able to reproduce the main pattern of Rossby waves in the observed climate. The negative anomaly over the North Pacific is centered approximately 10° too far west in the model, and the magnitudes of the low-level anomalies between 0° and 30°N are overestimated. These tropical biases may be the result of errors in diabatic heating in the northeast Pacific ITCZ; the CTL simulation has significant precipitation biases in the deep tropics relative to the Global Precipitation Climatology Project dataset (Adler et al. 2003), particularly over the eastern Indian Ocean and in the Pacific ITCZ. North of 20°N , the model reproduces the spatial distribution and magnitude of observed precipitation fields well. The overestimation of the low-level tropical ψ' does not extend to 250 mb.

Figures 4a, 4b, 4g, and 4h show low-level θ and upper-level U in ERA-Interim and CTL. The model reproduces the spatial patterns of low-level θ well, although with slightly higher low-level temperatures over northeast Asia and in the polar region, reducing the meridional temperature gradient to the south of these regions. Upper-level U is reproduced well, with the Pacific jet well simulated in both location and strength, although with a slightly greater southwest–northeast tilt than in ERA-Interim. The vertical structure of zonal wind over the jet region is also well simulated, with the jet magnitude peaking between 150 and 250 mb (not shown).

3. Impact of combined Tibetan and Mongolian Plateaus

The impact of the combined Tibetan and Mongolian Plateaus on circulation is shown in Figs. 3c and 3i (lower and upper levels, respectively). The orography induces a low-level anticyclonic ψ' anomaly to the north and northwest of the orography, a weak cyclonic anomaly to the southwest, and a downstream wavelike response.

Comparison to the theoretical responses depicted in Fig. 1 suggests the orography blocks most of the impinging flow, deflecting it horizontally. Analysis of vertical velocity changes suggests that some vertical deflection is also occurring (not shown). The response is consistent with the response to idealized orography found by Brayshaw et al. (2009) and Saulière et al. (2012). The centers of action of the upper-level anomalies are shifted westward relative to the low-level anomalies, consistent with the vertical propagation of Rossby waves.

Comparison of Figs. 3h and 3i suggests that the Tibetan and Mongolian Plateaus together are responsible for approximately half the total DJF ψ' over eastern Eurasia and the Pacific Ocean (note the change in color scales from the CTL and ERA-Interim figures). This is broadly consistent with the stationary wave model results of Held et al. (2002), who find that approximately one-third of the wintertime ψ' is from orography, with diabatic heating contributing to the remaining two-thirds.

The flux vectors overlain on the upper-level panels show the Takaya–Nakamura propagation of wave activity. Over the Pacific, the wave activity is largely confined to a latitude band spanning approximately 20° – 55°N ; equatorward propagating wave energy is refracted in the central Pacific toward the pole and then back toward the equator again when the wave train reaches Western North America. Such confinement can be thought of as the response to a waveguide, as discussed by Hoskins and Ambrizzi (1993).

The circulation induced by the orography affects θ , shown at 850 mb in Fig. 4c. The warming to the northwest and cooling to the east of the plateaus are consistent with the anomalous southerly and northerly flow depicted in Fig. 3c.

Figure 4i shows the change in upper-level U from the combined orography. Consistent with the streamfunction changes in Fig. 3i, there is a strong increase in zonal wind in the western Pacific at $\sim 30^\circ$ – 50°N . This amounts to a $\sim 25\%$ increase in the strength of the Pacific jet. The orography shifts the jet slightly northward, and, as found by Brayshaw et al. (2009), the increase in U due to orography has a slight southwest to northeast tilt. The decrease in zonal wind over Asia between 40° and 60°N is consistent with the increase in surface friction and gravity wave drag over the mountain. The orography-induced increase in U extends from the surface to ~ 100 mb, peaking in amplitude at ~ 250 mb.

4. Mongolian Plateau versus Tibetan Plateau

a. Circulation impacts

We now consider the impacts of the Mongolia and Tibetan Plateaus separately (Figs. 3d,e and 3j,k). Figures 3d and 3j show that the Mongolian Plateau by

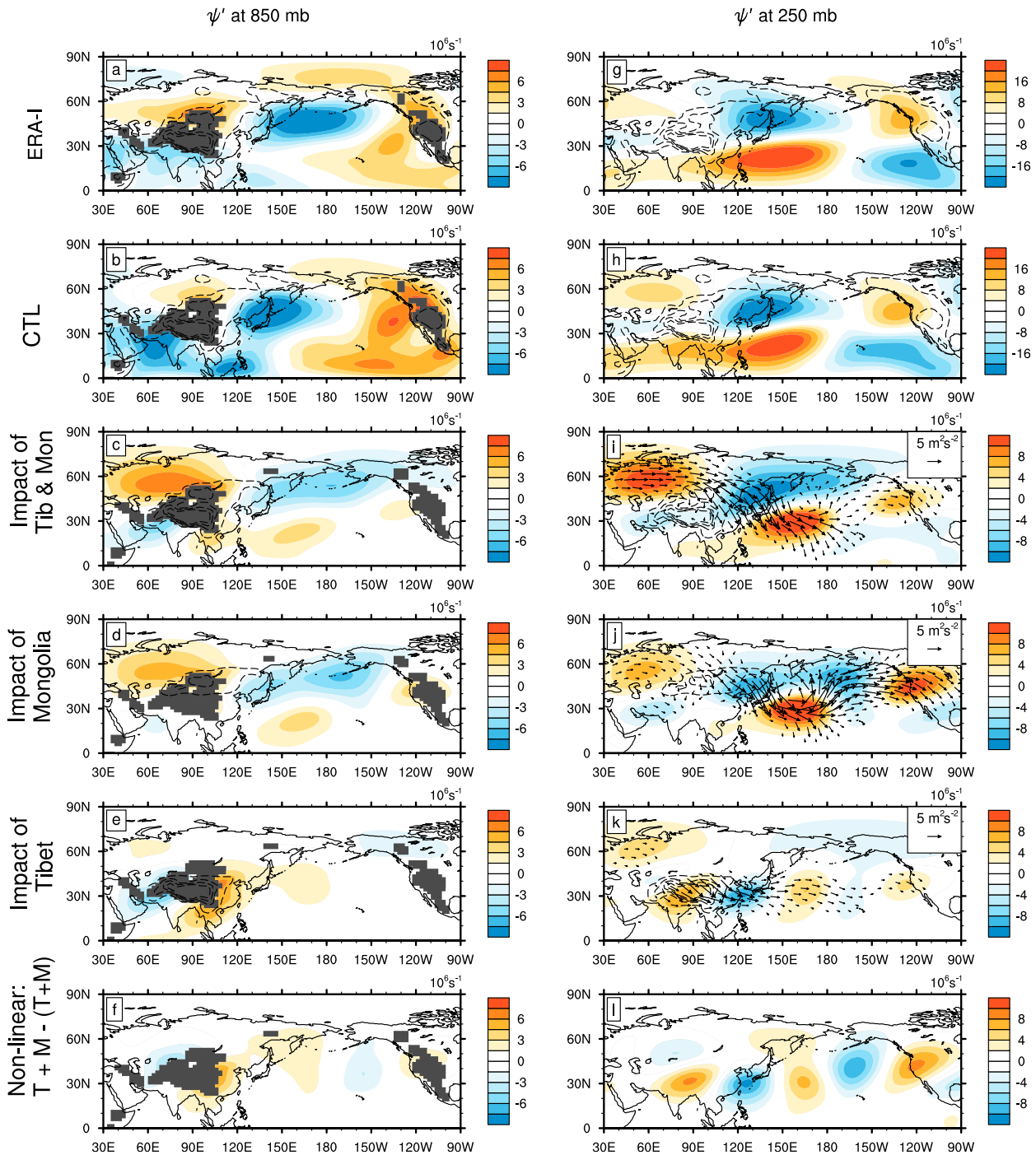


FIG. 3. Climatological DJF ψ' (10^6 s^{-1}) at (left) 850 mb and (right) 250 mb for realistic-orography experiments with fixed SSTs. (a),(g) ERA-Interim values; (b),(h) values from the CTL simulation. Other panels show the impact of orography (i.e., CTL minus experiment) for (c),(i) the Tibetan and Mongolian Plateaus combined; (d),(j) the Mongolian Plateau; and (e),(k) the Tibetan Plateau. (f),(l) The nonlinearity of combining the two individual orographic responses [e.g., (f) = (d) + (e) - (c)]. (i)–(k) Vectors show fluxes of wave activity ($\text{m}^2 \text{ s}^{-2}$; see text). Dashed lines show contours of orography (or orographic difference) in 1000-m increments from 500 m. Regions are gray where the 850-mb surface lies below the boundary layer.

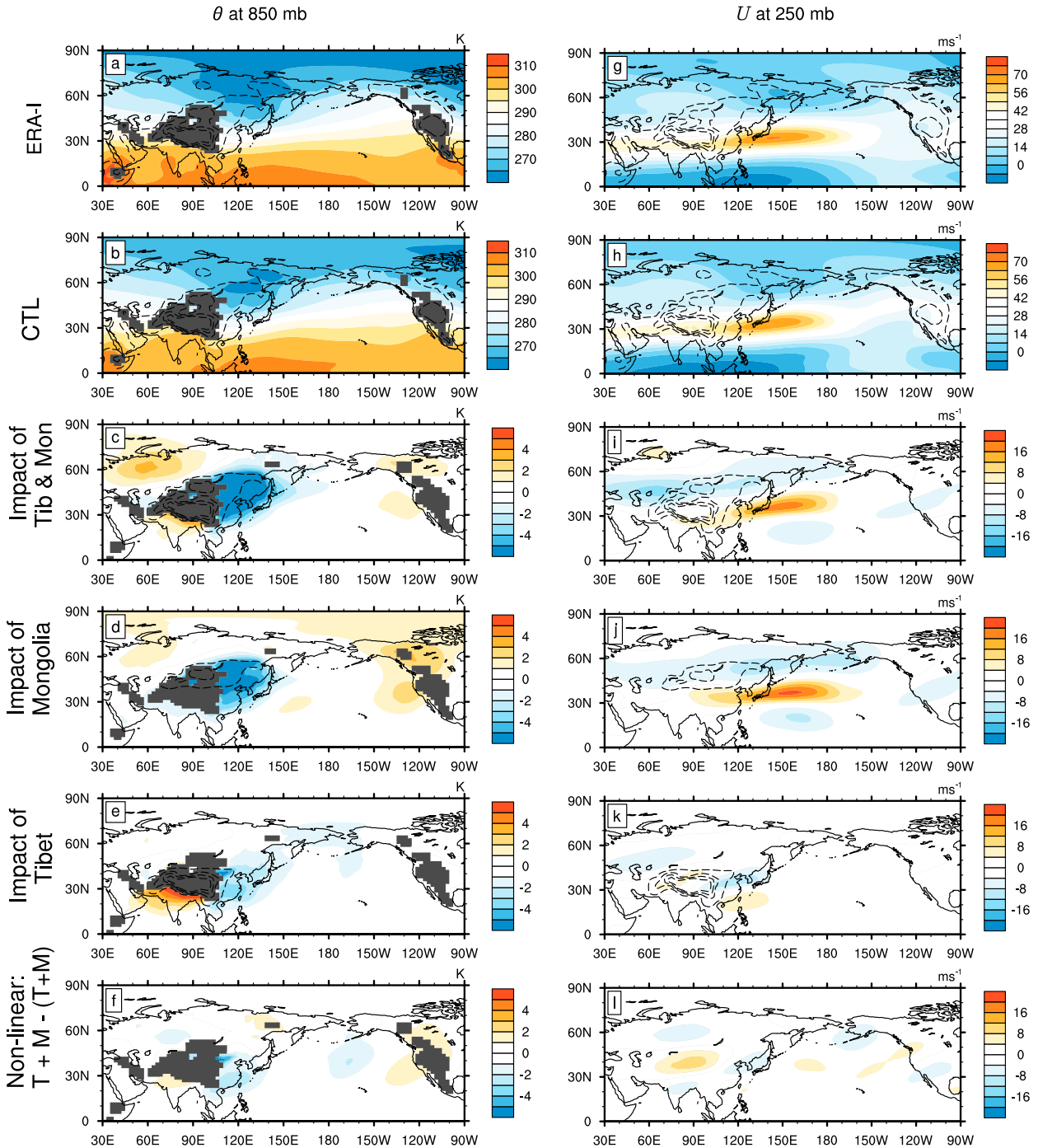


FIG. 4. As in Fig. 3, but for (left) θ at 850 mb (K) and (right) U at 250 mb (m s^{-1}).

itself produces a similar spatial pattern to the combined orography (Figs. 3c,i), albeit with generally weaker near-field amplitude. Conversely, the only similarity in spatial pattern between the response to the Tibetan Plateau and the combined response is the low-level near-field response equatorward of 45°N. This suggests that, while the larger Tibetan Plateau has an impact in the

immediate vicinity of the orography, it is the Mongolian Plateau that has the strongest impact on far-field circulation.

The low-level response to the Mongolian Plateau has a positive lobe to the northwest of the orography, similar to the horizontal-deflection-dominated response of the combined orography. Conversely, the response to

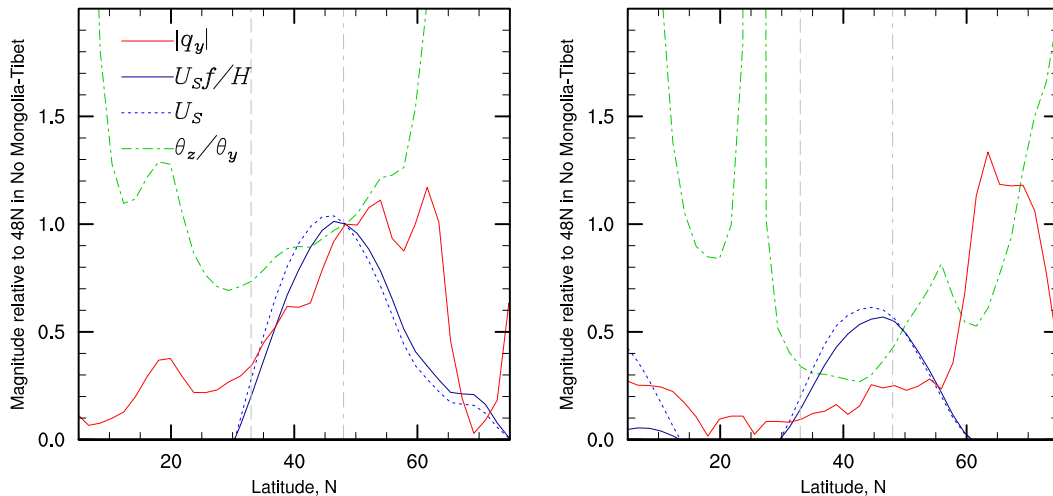


FIG. 5. (a) Meridional variations in the climatological forcing terms for vertical deflection (solid blue), horizontal deflection (solid red), U component of vertical deflection (dotted blue), and θ_z/θ_y (green dotted–dashed line) for the no Tibet and Mongolia simulation in DJF. (b) As in (a), but for AMJ. Variables are calculated as means between 925 and 850 mb and 60° and 100°E . All variables are shown relative to their magnitude at 48°N in DJF for the no Tibet and Mongolia experiment (a). The vertical dashed gray line shows the approximate latitude of centroid of the Tibetan Plateau; the dotted–dashed gray line that for the Mongolian Plateau.

the Tibetan Plateau shows an east–west dipole, with a positive lobe to the east and a negative lobe to the west; this has the opposite sign to a vertical-deflection response (see Fig. 1a). This different response may be due to the zero line in zonal wind, which lies around 30°N at 925 mb, or the presence of the Mongolian orography to the north in these experiments.

Figures 3f and 3l show the nonlinearity of adding the orography together: that is, impact of Tibet plus impact of Mongolia minus impact of combined Tibet and Mongolia. This field would be zero if the separate impacts of Mongolian and Tibetan orography combined linearly. The nonlinearity in ψ' looks similar to the response to the Tibetan Plateau. This suggests that the presence of Mongolia strongly dampens the response to Tibet, while the presence of Tibet has relatively little impact on the response to Mongolia.

Figures 4j and 4k show that the Mongolian Plateau causes a strong increase in the upper-level jet, with a maximum value of $\sim 20\text{ m s}^{-1}$, while the Tibetan Plateau results in a maximum increase of only $\sim 5\text{ m s}^{-1}$, consistent with the ψ' responses.

b. Response amplitude

Theory predicts that the amplitude of a vertical-deflection response to forcing should scale as $(f/H)\mathbf{u}\cdot\nabla h$, while that of a horizontally deflected response should scale as $q_y\eta$. Hence, for a fixed-shape mountain (i.e., fixed ∇h and η), we can estimate how the amplitude of the vertical and horizontal-deflection responses will vary with

the latitudinal position of the orography by plotting $(f/H)U$ and q_y as a function of latitude, shown in Fig. 5. Values shown are averages from 60° to 100°E and 925 to 850 mb, approximately representing the flow impinging on the orography; results are insensitive to the details of the longitude and pressure ranges. Values in all plots are shown as a fraction of the magnitude at 48°N in DJF for the no Mongolia and Tibet simulation, which approximates the flow into which the Tibetan or Mongolian Plateau is placed. In all plots, the meridional variation in forcing from vertical deflection $(f/H)U$ is dominated by the variation in U (dashed blue).

For DJF in the no Mongolia and Tibet simulation (Fig. 5a), the response magnitude for vertical deflection (solid blue) is maximum at $\sim 46^\circ\text{N}$, while the response magnitude for horizontal deflection (solid red) has peaks at $\sim 54^\circ$ and $\sim 62^\circ\text{N}$. Thus, theory predicts that the Mongolian Plateau, centered at $\sim 48^\circ\text{N}$, is close to optimally placed for near-maximum forcing magnitude regardless of whether the forcing is vertical or horizontal deflection, and perhaps particularly when it is a combination of the two. The Tibetan Plateau is both higher (by a factor of ~ 2.5) and meridionally more extensive (by a factor of ~ 1.5) than the Mongolian Plateau; these differences in orographic size will counter some of the latitudinal differences in forcing.

Theory also predicts whether the response should be dominated by horizontal ($\theta_z h/|\theta_y \eta| > 1$) or vertical ($\theta_z h/|\theta_y \eta| < 1$) deflection. At 48°N , $\theta_z/\theta_y \sim 1000$. For the Mongolian orography, taking $h \sim 2\text{ km}$ and $\eta \sim 600\text{ km}$

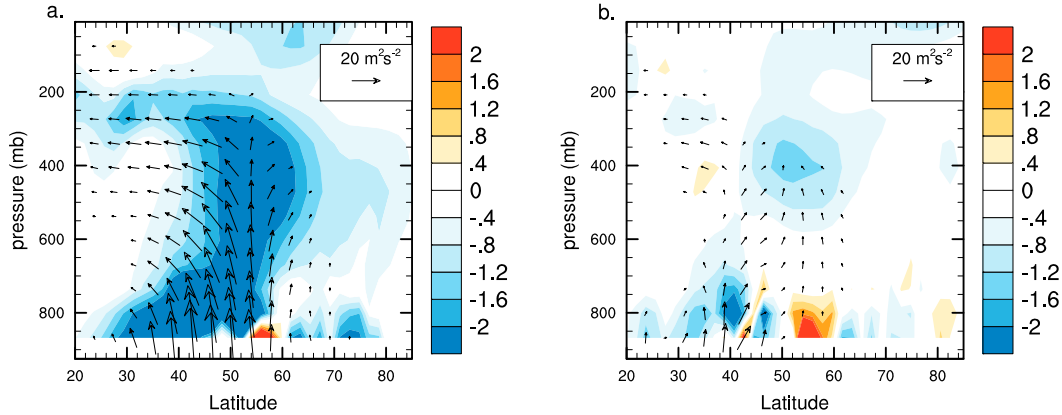


FIG. 6. EP fluxes ($\text{m}^2 \text{s}^{-2}$; vectors) and divergence (m s^{-2} ; contours) for DJF: (a) impact of Mongolian Plateau and (b) impact of Tibetan Plateau. Scaling is applied as described in section 2, including a scaling of the divergence field by $1/(a \cos \phi)$.

(see Fig. 2), the response to the Mongolian orography should be more horizontal deflection than vertical deflection, as $\theta_z h / \theta_y \eta \sim 3$. This is consistent with the spatial pattern of response seen in Figs. 3d and 3j. For the Tibetan Plateau, $h \sim 5 \text{ km}$, $\eta \sim 1000 \text{ km}$, and $\theta_z / \theta_y \sim 750$; we again find that horizontal deflection should dominate, as $\theta_z h / \theta_y \eta \sim 4$. This does not match the simulated response; however, as discussed in section 4a, the response may be complicated by the zero line in low-level U at $\sim 30^\circ \text{N}$ or the presence of other orography.

Examination of EP fluxes provides a perspective on the vertical and meridional propagation of wave energy from a source. Figure 6 shows the differences in the stationary wave EP fluxes, and their divergence, in response to the Mongolian and Tibetan Plateaus separately. Energy propagates vertically away from the source region and then turns toward the equator at upper levels. Comparison of vector magnitudes at lower levels shows clearly that Mongolia (Fig. 6a) is a much larger source of wave energy to upper levels than Tibet (Fig. 6b).

The response of the downstream circulation, including the jet response, will also be affected by the propagation of this wave energy downstream of the orography, which we now discuss.

c. Rossby wave trains

The largest response in upper-level U is located at approximately 38°N , a latitude occupied by the Tibetan Plateau. This may have contributed to the widespread assumption that the Tibetan Plateau has the largest impact on the jet. This momentum change can be understood as features of a stationary Rossby wave; an increase in zonal wind requires a negative meridional gradient in anomalous geopotential ($f\Delta U \approx -\partial\Delta\Phi/\partial y$). In this section, we examine differences in the propagation

paths for Rossby waves forced by the Mongolian and Tibetan orography individually and consider how such differences may impact the zonal jet response.

The wave-activity flux vectors for both the Mongolian and Tibetan Plateaus show evidence of propagating stationary waves, largely confined within a given latitude band (Figs. 3j,k). Orography-induced Rossby wave trains with equatorward paths, as seen immediately downstream of the plateaus, are consistent with previous work (e.g., Hoskins and Karoly 1981; Valdes and Hoskins 1991), and a meridionally confined response is consistent with waveguide behavior (e.g., Hoskins and Ambrizzi 1993). Figure 7a shows upper-level K_s ; a strong Rossby waveguide created by a local maximum (in the meridional direction) in K_s can be seen at $\sim 25^\circ\text{--}35^\circ \text{N}$. There is also a much weaker waveguide at $\sim 45^\circ\text{--}55^\circ \text{N}$.

Figure 3j suggests that the initial Rossby wave excited by the Mongolian Plateau has a zonal wavenumber of $k \sim 2.5$ (based on the first two ψ' anomalies, i.e., half a wavelength, at $\sim 60^\circ$ and $\sim 130^\circ \text{E}$, respectively). As there is little circumglobal propagation of the response, the dominant wavenumbers do not need to be integer values; k and l are calculated as inversely proportional to the local wavelength. We now consider the theoretical response to a $k = 2.5$ wave excited at the location of the Mongolia Plateau (centroid given approximately by the white circle in Fig. 7a), where $K_s \sim 3.5$. Initially, as $k < K_s$, $l \approx \pm 2.5$, and thus the excited waves will propagate both zonally and meridionally. As the equatorward-propagating wave travels into the local minimum in K_s around 40°N it will be refracted toward more zonal propagation. Any wave activity that is able to reach the southward side of this local minimum will see a gradient of $\partial K_s / \partial y < 0$; l will therefore increase in magnitude, and the wave will be refracted toward the south and into the

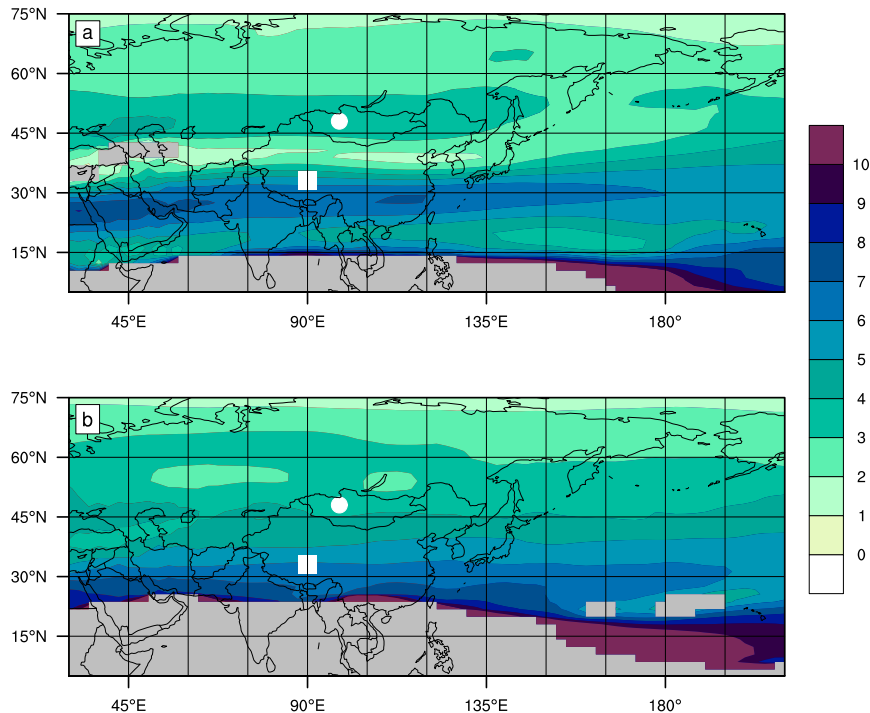


FIG. 7. Stationary wavenumber K_s at 250 mb for: (a) DJF and (b) AMJ for the no Tibet and Mongolia experiment with fixed climatological SSTs, 40-yr mean.

strong waveguide in the jet region. Wave activity that does not cross the local K_s minimum here may still be refracted southward into the jet waveguide as the minimum reduces in magnitude toward 135°E . Once south of the maximum in K_s at $\sim 30^\circ\text{N}$, l will decrease in magnitude as the wave travels southward into the lower K_s environment, and the wave will be refracted back toward a more zonal propagation. This simplified view neglects impacts of zonal changes on k and assumes that a single wavenumber of k is excited by the orography; despite these simplifications, the wave activity fluxes in Fig. 3j are qualitatively consistent with this picture. The wave activity fluxes suggest some southward crossing of the local minimum at 40°N , although the majority of the southward propagation at this latitude occurs east of 135°E , where the strength of the minimum is much reduced.

We now consider the theoretical response to a wave source at the location of the Tibetan Plateau (centroid given approximately by the white square in Fig. 7a). Figure 3 suggests an initial zonal wavenumber of $k \sim 4$ (based on the positive ψ' anomalies at $\sim 80^\circ$ and $\sim 170^\circ\text{E}$; we do not consider the anomaly at $\sim 60^\circ\text{E}$, 60°N as part of the main forced wave). At the Tibetan Plateau, $K_s \sim 5.5$. Thus, initially $|l| \approx \pm 3.5$, and the response will have significant meridional propagation. Any poleward wave activity will be rapidly refracted toward the equator by

the strong meridional gradient in K_s in which the Tibetan Plateau sits. Any northward propagation will be limited beyond the latitude at which $K_s = k \sim 4$: that is, approximately 35°N over the Asian Continent. Downstream propagation will be meridionally trapped within the strong waveguide. Any initially equatorward traveling wave will also be trapped within this waveguide. Overall, this response has limited northward propagation away from the source, qualitatively consistent with the wave activity fluxes in Fig. 3k.

As noted above, an increase in zonal wind requires a negative meridional gradient in anomalous geopotential. Following the streamfunction patterns in Fig. 3i and 3j, we find that the average propagation path of Rossby waves forced by the Mongolian Plateau results in substantial meridional gradients over the Pacific, resulting in strong changes to the zonal wind. Conversely, the strong meridional confinement of the waves from the Tibetan Plateau results in weaker meridional gradients and thus smaller changes in U .

d. Storm-track response

In addition to changes in circulation, there are large changes in storminess over the Pacific with the presence of orography, as measured by the time variability of 2–6-day Lanczos-filtered 250-mb geopotential height (following Brayshaw et al. 2009). The Mongolian Plateau

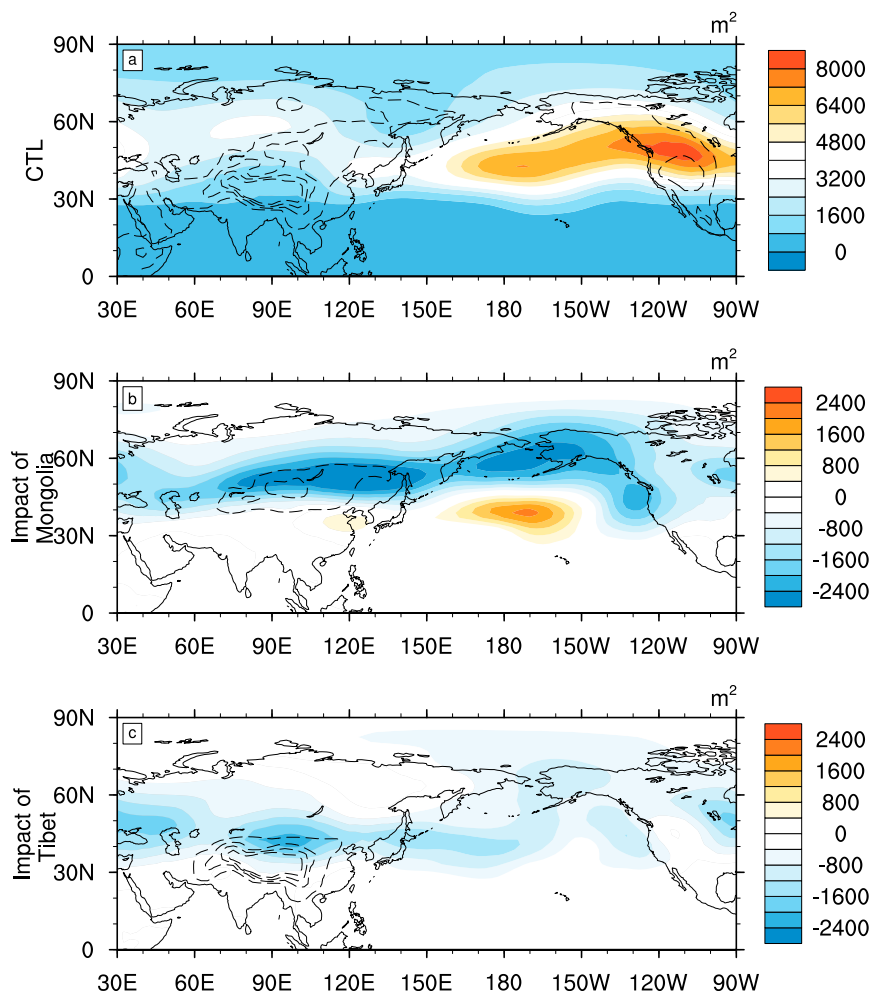


FIG. 8. Change in DJF storm-track strength as measured by the time variability of 2–6-day Lanczos-filtered 250-mb geopotential height. (a) CTL simulation, (b) impact of Mongolia, and (c) impact of Tibet. Dashed contours are as in Fig. 3.

causes an increase in storminess in the central Pacific storm-track region of up to 30%, with decreases in storminess to the north and over land (Fig. 8a). The response to the Tibetan Plateau includes a decrease in storminess of approximately 20% in the central Pacific storm track (Fig. 8b).

e. Seasonal cycle

We briefly investigate the impact of orography in months outside of Northern Hemisphere winter. Following Zappa et al. (2015), we group months not by predefined seasons, but by similarity of the dynamical response. In the shoulder winter months, October–November and March, the response to the Mongolian Plateau has a very similar spatial distribution to the response in DJF, but the magnitude of the response is smaller, likely because of smaller values of low-level q_y and U at the latitude of Mongolia in these months (see

Fig. 5b and discussion in section 4b). Similar to DJF in these shoulder winter months, we find the ψ' response to the Tibetan Plateau is largely zonal, and thus there is little impact on the zonal jet. This is to be expected, as the strong meridional gradient in K_s at the latitude of Tibet exists from October through March, preventing substantial meridional propagation of the forced waves.

In April–June, the upper-level ψ' response to the combined orography (Fig. 9) is similar in pattern but reduced in magnitude by up to 50% relative to that in DJF (cf. Figs. 9a and 3i). Interestingly, the individual plateau responses show that in this season the combined response is largely due to the Tibetan Plateau (Figs. 9b,c). Correspondingly, the Mongolian Plateau has little impact on the zonal jet in April–June (AMJ), while the Tibetan Plateau produces an increase in 250-mb zonal wind of up to 14 m s^{-1} (not shown). For the Mongolian Plateau, we can explain the reduced response magnitude by the

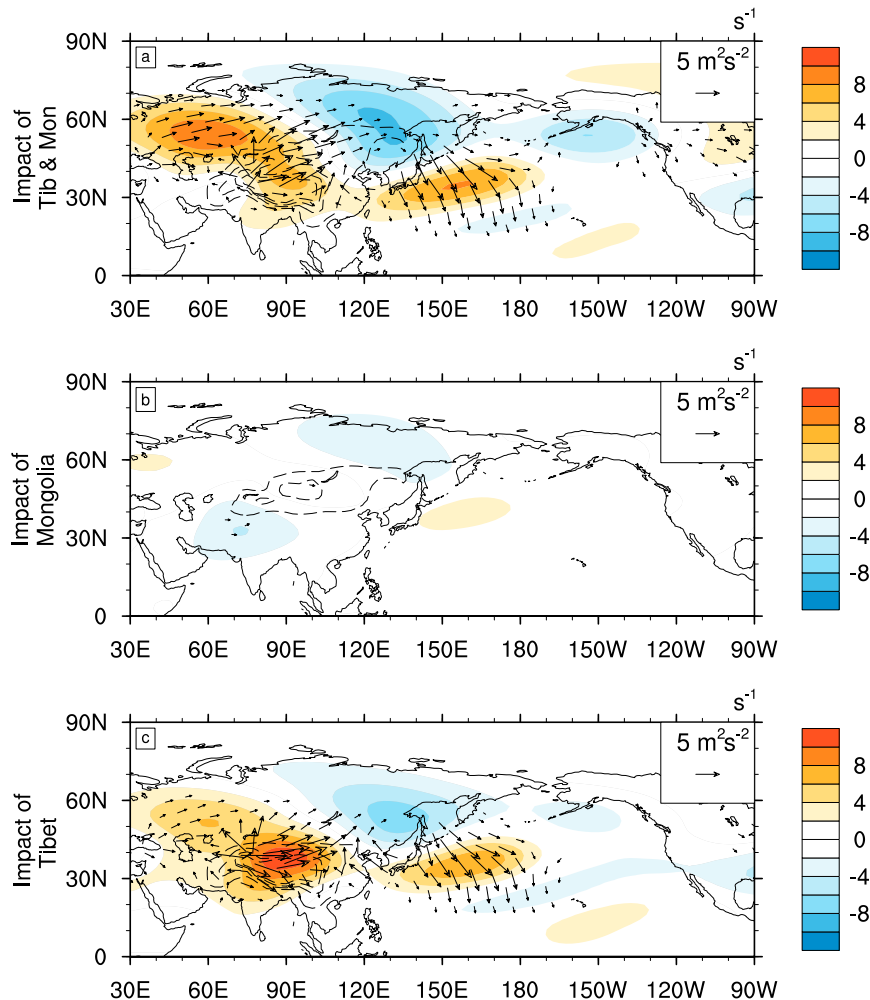


FIG. 9. Change in climatological ψ' (10^6 s^{-1}) at 250 mb in April–June. (a) Impact of combined Mongolia and Tibetan orography, (b) impact of Mongolia, and (c) impact of Tibet. Vectors and dashed contours are as in Fig. 3.

smaller values of low-level q_y and U at the latitude of Mongolia in AMJ relative to DJF (cf. Figs. 5a and 5b). For the Tibetan Plateau, the AMJ response has a different spatial pattern to DJF, with much more meridional propagation in AMJ. Comparison of K_s between DJF and AMJ (cf. Figs. 7a and 7b) shows much weaker meridional gradients between 25° and 50°N in AMJ. The northward limit of waves excited by the Tibetan orography, set by $K_s = k \sim 4$, is now at $\sim 45^\circ\text{N}$, in contrast to $\sim 35^\circ\text{N}$ in DJF, allowing greater meridional propagation of the forced waves and thus a greater impact on the zonal wind.

f. Some sensitivity experiments

The main conclusions of this section are unchanged when the atmosphere is coupled to a slab-ocean lower boundary instead of fixed SSTs. This suggests that orographically modified downstream surface fluxes play a

secondary role in the response of the atmosphere to Asian orography.

We performed the CTL, no Mongolian Plateau, and no Tibetan Plateau experiments with the MPI-ESM ECHAM6 coupled to a slab ocean (Stevens et al. 2013) at T63 spatial resolution (approximately $2^\circ \times 2^\circ$) for 10 simulation years. The results obtained are similar to those shown for the CAM4: the Mongolian Plateau has a much larger circulation response than the Tibetan Plateau in DJF, while the Tibetan Plateau predominates in AMJ.

5. Idealized plateau experiments

a. Mongolian Plateau versus Tibetan Plateau

We now show that the main results from the previous section can be qualitatively reproduced using idealized

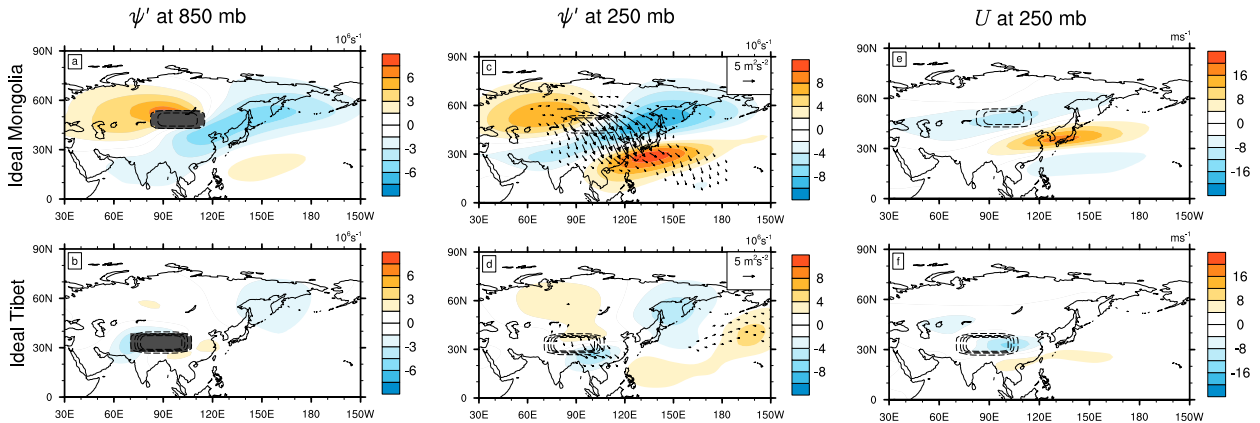


FIG. 10. Streamfunction anomaly ψ' (left) at 850 mb and (center) at 250 mb (10^6 s^{-1}) and (right) U at 250 mb (m s^{-1}) for idealized plateau experiments with fixed SSTs. Vectors, dashed contours, and gray shading are as in Fig. 3. (a),(c),(e) Impact of idealized Tibetan Plateau; (b),(d),(f) impact of idealized Mongolian Plateau.

plateaus on an otherwise flat Earth. This tests the sensitivity of the response to the presence of other global orography and to the details of the orography added. In the idealized Tibetan Plateau experiment, the Tibetan Plateau is represented by a 5-km-high idealized plateau centered on 33°N and 92°E, while in the idealized Mongolian Plateau experiment, the Mongolian Plateau is represented by a 2-km-high idealized plateau centered on 48°N and 98°E. Both idealized plateaus have meridional widths of $\sim 16^\circ$ and zonal widths of $\sim 40^\circ$ at the base.

Figure 10 shows the lower- and upper-level ψ' and upper-level U anomalies produced by the idealized plateaus individually in DJF. The idealized Mongolian Plateau produces a response similar to the realistic Mongolian Plateau at both lower and upper levels (cf. Figs. 10a,c,e with Figs. 3d,j, 4j); however, immediately to the south of the idealized Mongolian Plateau there is a greater low-level response to the orography than there was to the realistic plateau (cf. Figs. 10a and 3d), perhaps as a result of interference from the Tibetan Plateau in the realistic-orography experiment. The magnitude of the zonal jet response is similar between the realistic and idealized Mongolian Plateaus (cf. Figs. 10d and 4j). The response to the idealized Tibetan Plateau (Figs. 10b,d,f) is weak relative to the response to Mongolian orography, as for the realistic experiments.

Unlike the realistic experiments, the wave-activity flux vectors show little waveguide trapping over the Pacific for both idealized experiments (Figs. 10c and 10d). This is despite very similar K_s fields between the idealized and realistic experiments (not shown).

b. Impact of idealized plateau latitude

We argued in section 4b that the Mongolian Plateau has a large impact on the Pacific jet because of its

placement within a large meridional potential vorticity gradient, near the latitude of maximum low-level zonal wind, and within a distribution of K_s that induces substantial equatorward propagation of the forced Rossby waves. To further investigate the impact of latitude on the response, we conduct a set of experiments in which the idealized Mongolian Plateau is moved north in $\sim 5^\circ$ latitude increments, from 43° to 63°N. The plateau has the same spatial footprint in kilometers in each of these experiments. We also performed these varying latitude experiments, but with the longitudinal arc-width of the plateau fixed (so holding the zonal wavenumber constant), and find very similar results to the fixed-width experiments shown here.

Figure 11 shows the lower- and upper-level ψ' and upper-level U anomalies for plateaus centered (from top to bottom) at 63°, 53°, and 43°N (note changes in color scale from previous figures). The maximum response is found for orography located at 48°–53°N; the response to a plateau at 53°N is practically indistinguishable from that at 48°N. Responses decrease in amplitude smoothly as the plateau latitude is moved poleward of 53°N or equatorward of 48°N. The increasing magnitude of θ_z/θ_y with latitude between 30°–60°N in the flat-CTL experiment (similar to that in the CTL experiment, shown by the green dotted–dashed line in Fig. 5a), suggests that the horizontal deflection component of the response should become stronger as the orography is moved farther north; however, it is difficult to discern from the response patterns in Fig. 11 whether this holds true in our experiments.

Between 100° and 150°E, the latitude of the response is relatively insensitive to the latitude of the mountain: the maximum of zonal jet increase varies by only $\sim 6^\circ$ latitude for the 20° change in plateau latitude (see

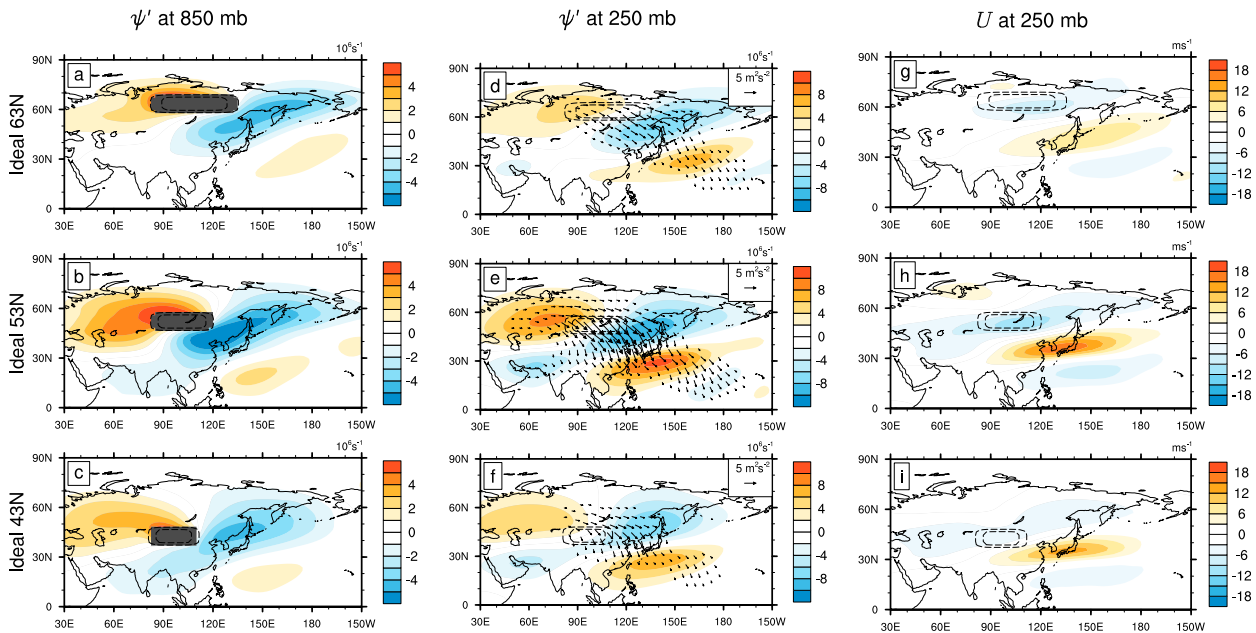


FIG. 11. As in Fig. 10, but for idealized orography experiments with fixed climatological SSTs, DJF 30-yr mean. (a),(d),(g) Idealized plateau at 63°N; (b),(e),(h) idealized plateau at 53°N; and (c),(f),(i) idealized plateau at 43°N.

Figs. 11g–i). This aspect of the response is discussed further in section 6.

A subset of these varying latitude experiments with idealized Mongolian orography was repeated with the CAM coupled to a slab ocean, with the idealized plateau placed 25° farther west, with the idealized orography placed in a no Mongolia and Tibet world (thus with other global orography included) and with a 1-km-high idealized plateau (thus looking at a vertically deflected response; see section 5c). In all cases, the impact of plateau latitude on response magnitude and response latitude remains similar to the results shown; in the westward shifted experiments the response, including the upper-level jet increase, shifts west with the orography.

c. Impact of idealized plateau height

Our results suggest that the Mongolian Plateau is close to ideally situated to have the strongest impact on the upper-level jet over the western Pacific. Here we investigate the importance of the height of an idealized plateau located in this sweet spot.

Figures 12a–c show the low-level ψ' for idealized plateaus of 1-, 2-, and 4-km height centered at 48°N. An experiment with a 6-km plateau has a response almost identical to that of the 4-km plateau. As plateau height increases, the strength of the response increases, and the spatial distribution of the lower-level circulation response differs significantly, from vertical deflection (1 km) through to almost pure horizontal deflection (4–6 km). The 2-km plateau response, with a northwest–southeast

dipole, is consistent with a combination of vertical and horizontal deflection.

The upper-level ψ' and U are shown in Figs. 12d–i. The strength of the near-field response increases with increasing plateau height, and the spatial distribution of circulation anomalies, and downstream wave propagation, changes. A strong waveguide effect is apparent only for the 4- and 6-km plateaus. The magnitude of the response in the 100°–180°E region is smallest for the 1-km plateau but very similar for the 2-, 4-, and 6-km cases. The increase in U extends farther east and has less southwest–northeast tilt between 100° and 180°W as plateau height is increased.

6. Discussion

We have sought to understand what aspects of Asian orography matter most for stationary waves in the wintertime circulation. Consistent with Shi et al. (2015), we find that, despite its smaller extent and height, the Mongolian Plateau has a much greater influence on the Pacific jet stream than the Tibetan Plateau. We attribute this to differences in the strength of the forcing—associated with latitudinal variations in low-level q_y and U —and in the propagation paths of the forced Rossby waves.

Vectors of phase-independent wave-activity flux suggest that the downstream response to realistic orography is meridionally confined within the waveguide produced by the strong meridional maximum in K_s in the jet region (e.g., Hoskins and Karoly 1981; Hoskins and Ambrizzi 1993).

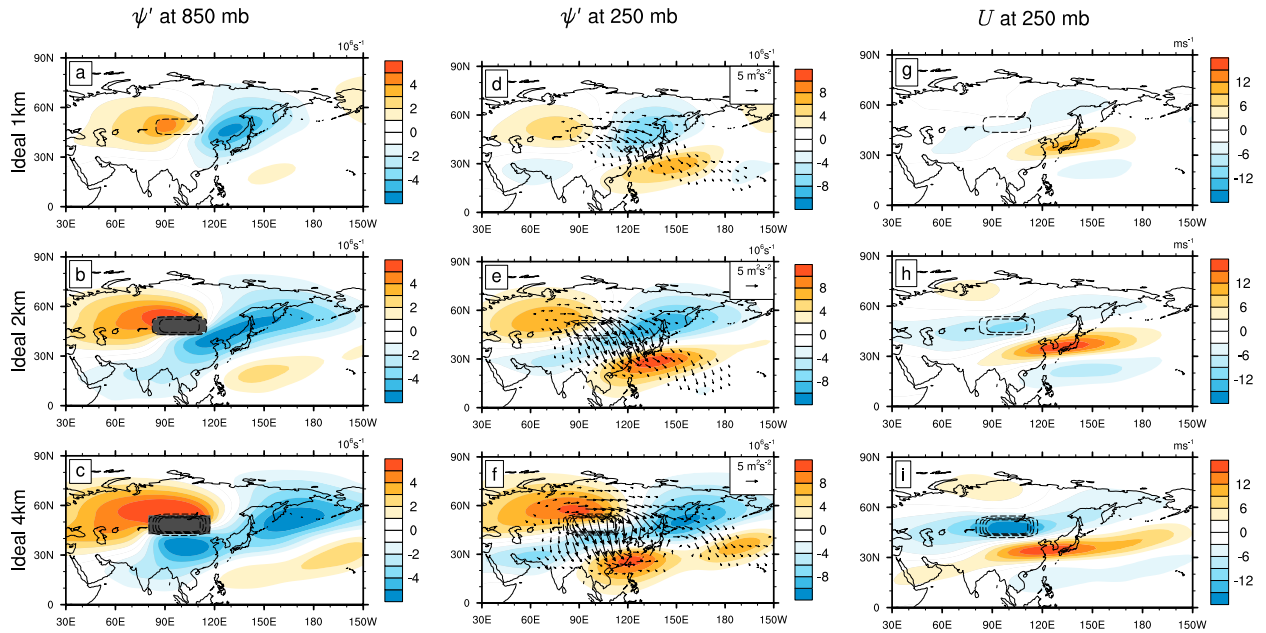


FIG. 12. As in Fig. 11, but for idealized plateaus of 1-, 2-, and 4-km height centered on 48°N.

The Mongolian Plateau is located $\sim 20^\circ$ north of this K_s maximum. Much of the orographically generated wave activity is refracted equatorward by the K_s meridional gradient toward and into the waveguide. This meridional propagation gives rise to large meridional gradients in ψ' and thus large changes in the zonal jet. Conversely, the Tibetan Plateau is located only $\sim 5^\circ$ north of the strong waveguide and within a strong meridional gradient in K_s . The strong gradient rapidly refracts any poleward-propagating waves southward into the waveguide, inhibiting any propagation north of $\sim 35^\circ$ N. Limiting the meridional propagation reduces the ability of the wave to create meridional gradients in ψ' and thus limits their impact on U . Such zonally oriented patterns are similar to the circumglobal teleconnections seen in reanalysis data (e.g., Branstator 2002). For the idealized plateaus, waveguide Rossby wave trapping occurs only for plateaus of 4-km height or greater.

The circulation response to orography in months outside of DJF is consistent with our conclusions of the importance of low-level q_y and U and on background K_s . Months that have weaker low-level q_y and U at the latitude of the Mongolian Plateau show weaker atmospheric responses. Conversely, the magnitude of the zonal jet response to Tibet peaks in April–June, reaching $\sim 60\%$ of the magnitude of the Mongolian Plateau DJF response. We attribute this to the weaker meridional gradient in K_s in the vicinity of Tibet in April–June, which allows Rossby waves forced by the Tibetan Plateau to propagate much farther northward than in DJF

before being refracted back southward into the waveguide. The resulting meridional propagation leads to meridional gradients in ψ' and thus changes in the zonal jet. This is consistent with the results of Manola et al. (2013), who find that faster, narrower jets (i.e., in DJF) are more likely to trap Rossby wave energy.

The latitude of an idealized plateau is found to have a strong influence on the magnitude of the jet stream response, but only a small influence on the latitude of the jet response, for orography centered between 43° – 63° N. This insensitivity of response latitude to forcing latitude requires the Rossby wave phase change (from negative to positive geopotential) to be located farther south relative to the orography for a plateau located farther north. North of $\sim 48^\circ$ N, K_s decreases toward the pole (see Fig. 7a). Assuming the same zonal wavenumber k is excited by the orography at all latitudes, the relation $K_s^2 = k^2 + l^2$ shows that more northerly generated waves should therefore have a lower initial l . They should thus propagate more zonally and have a larger meridional wavelength than waves generated at lower latitudes. This will result in different ray paths, which appear to partially compensate for the northward shift of the plateau (wave source).

We find that increases in elevation above 2 km have only a muted impact on the maximum strength of the zonal jet response. This is consistent with the dominance of horizontal deflection over vertical deflection for mountains above ~ 2 km and the scaling of the horizontal-deflection response as $q_y \eta$, which is independent of

mountain height. The jet response extends farther eastward as the orographic height is increased. This change in eastward extent may influence the steering of storms and weather events; however, the eastward extent is likely sensitive to the extent of waveguide trapping of Rossby waves, which varies between the idealized and realistic responses.

Consistent with previous studies (e.g., Brayshaw et al. 2009; Saulière et al. 2012), we find an increase in central Pacific storm-track strength in response to the Mongolian Plateau of up to 30%. Conversely, the Tibetan Plateau decreases storm-track strength in this region by up to 20%.

Throughout this paper we concentrate on tropospheric effects; however, the presence of the orography reduces zonal wind speed in the midlatitude stratosphere (not shown), consistent with the time-averaged effects of sudden stratospheric warmings (SSWs; Matsuno 1971). Analysis of monthly data suggests that the removal of orography reduces the annual frequency of SSWs from approximately 1 event every 2 years in the CTL simulation to 1 event every 12–14 years when either the Tibetan Plateau or Mongolia Plateau are removed. We caution, however, that the region above 30 mb is damped in this AGCM; simulations with improved resolution in the stratosphere are required to fully understand the impacts of individual orographic ranges on stratospheric circulation and SSWs.

It is important to consider whether these modeling results are applicable to the real world. Comparison to ERA-Interim results (not shown) suggests that the CESM reproduces the observed key variables for the forcing (i.e., low-level q and U) quite well, as well as the upper-level distribution of K_s . This provides confidence that our realistic-orography results are applicable to the real world. Additionally, the importance of Mongolia is consistent with plots of observed stationary wave EP fluxes, which show the majority of the zonal-mean flux emanating from around 45°N (e.g., Edmon et al. 1980). These observed values will also be influenced by other global orography and by land–sea contrasts; however, comparison of the magnitudes of stationary EP fluxes for our CTL and no Mongolian Plateau experiments suggest that the Mongolian Plateau produces around 60% of the total zonal-mean EP-flux amplitude below 600 mb.

Our results may have interesting applications for paleoclimate studies, as the orography in the Mongolian Plateau region emerged much later than the Tibetan Plateau (Molnar and Stock 2009). For comparison with paleoclimate data local responses in both winds and precipitation must be considered (Sha et al. 2015), along with the seasonal variations we find.

Finally, one important question remaining is how the absolute and relative impacts of the Mongolian and

Tibetan Plateaus may vary as a function of mean-climate state. Our results suggest that the zonal jet response to orography is sensitive to any forcing that changes the background gradient in q , impinging zonal wind, and/or spatial distribution of K_s . Examples of such forcing include different orbital insolation, the presence/absence of extensive ice sheets, or climates with different equator–pole temperature gradients.

7. Conclusions

We perform atmospheric GCM experiments to show that the stationary waves and strengthening of the Pacific wintertime jet produced by Asian orography are predominantly due to orography located between 38.0° and 60.0°N, encompassing the Mongolian Plateau and the Altai, Hangayn, Tien Shan, Sayan, Baykai, and Hentiyn Mountain Ranges. The result holds true in both the CAM4 and ECHAM6 atmospheric GCMs. This contrasts with the long-held assumption that the Himalaya Mountain Range and Tibetan Plateau have the largest impact on atmospheric circulation.

The Mongolian Plateau is found to be ideally situated in a sweet spot of strong low-level meridional PV gradient and strong surface zonal wind such that the orography acts as a strong source of Rossby waves. Over the western Pacific these waves propagate to the southeast, creating an anomalous meridional geopotential gradient that intensifies the Pacific zonal jet. Conversely, the Tibetan Plateau forces smaller-amplitude Rossby waves that appear to be strongly meridionally confined in a waveguide; they therefore exhibit very little meridional propagation and thus have little impact on the jet. The relative importance of the two orographic regions differs in seasons outside of winter as a result of both differences in forcing strength and in the refraction of the excited Rossby waves.

Interestingly, simulations with idealized orography find that the latitude of the jet response over the western Pacific shifts by only 6° latitude in response to a plateau shift of 20° latitude. We propose that this is because of the decrease in K_s with increasing latitude north of ~45°N.

Orography exerts an important control on regional climate. This study has demonstrated an instance in which the stationary wave response is more sensitive to the latitude of large-scale orography than to orographic height. Our results may help provide new perspectives on interannual variability in stationary wave patterns, predictions of stationary wave responses to anthropogenic climate forcing, and atmospheric circulation patterns under the different geographic and orographic conditions of past climate states.

Acknowledgments. The authors thank David Brayshaw, Peter Molnar, and Brian Hoskins for stimulating conversation and/or constructive comments on the manuscript, as well as two anonymous reviewers for their helpful comments and feedback. RHW was supported by a Royal Society International Exchange Award, IE131056; the Joint Institute for the Study of the Atmosphere and Ocean, and Atmospheric Sciences department, at the University of Washington; and Imperial College London. DSB and GHR were supported by the National Science Foundation Division of Earth Sciences Continental Dynamics Programs, Awards 0908558 and 1210920. The CESM project is supported by the National Science Foundation and the Office of Science (BER) of the U.S. Department of Energy.

REFERENCES

- Adler, R. F., and Coauthors, 2003: The Version-2 Global Precipitation Climatology Project (GPCP) Monthly Precipitation Analysis (1979–present). *J. Hydrometeorol.*, **4**, 1147–1167, doi:[10.1175/1525-7541\(2003\)004<1147:TVGPCP>2.0.CO;2](https://doi.org/10.1175/1525-7541(2003)004<1147:TVGPCP>2.0.CO;2).
- Andrews, D. G., and M. E. McIntyre, 1976: Planetary waves in horizontal and vertical shear: The generalized Eliassen–Palm relation and the mean zonal acceleration. *J. Atmos. Sci.*, **33**, 2031–2048, doi:[10.1175/1520-0469\(1976\)033<2031:PWIHAV>2.0.CO;2](https://doi.org/10.1175/1520-0469(1976)033<2031:PWIHAV>2.0.CO;2).
- Boos, W. R., and Z. Kuang, 2010: Dominant control of the South Asian monsoon by orographic insulation versus plateau heating. *Nature*, **463**, 218–222, doi:[10.1038/nature08707](https://doi.org/10.1038/nature08707).
- Branstator, G., 2002: Circumglobal teleconnections, the jet stream waveguide, and the North Atlantic Oscillation. *J. Climate*, **15**, 1893–1910, doi:[10.1175/1520-0442\(2002\)015<1893:CTTJSW>2.0.CO;2](https://doi.org/10.1175/1520-0442(2002)015<1893:CTTJSW>2.0.CO;2).
- Brayshaw, D. J., B. Hoskins, and M. Blackburn, 2009: The basic ingredients of the North Atlantic storm track. Part I: Land–sea contrast and orography. *J. Atmos. Sci.*, **66**, 2539–2558, doi:[10.1175/2009JAS3078.1](https://doi.org/10.1175/2009JAS3078.1).
- Broccoli, A., and S. Manabe, 1992: The effects of orography on midlatitude Northern Hemisphere dry climates. *J. Climate*, **5**, 1181–1201, doi:[10.1175/1520-0442\(1992\)005<1181:TEOOM>2.0.CO;2](https://doi.org/10.1175/1520-0442(1992)005<1181:TEOOM>2.0.CO;2).
- Charney, J. G., and A. Eliassen, 1949: A numerical method for predicting the perturbations of the middle latitude westerlies. *Tellus*, **1**, 38–54, doi:[10.3402/tellusa.v1i2.8500](https://doi.org/10.3402/tellusa.v1i2.8500).
- Cook, K. H., and I. M. Held, 1992: The stationary response to large-scale orography in a general-circulation model and a linear model. *J. Atmos. Sci.*, **49**, 525–539, doi:[10.1175/1520-0469\(1992\)049<0525:TSRTLS>2.0.CO;2](https://doi.org/10.1175/1520-0469(1992)049<0525:TSRTLS>2.0.CO;2).
- Dee, D. P., and Coauthors, 2011: The ERA-Interim reanalysis: Configuration and performance of the data assimilation system. *Quart. J. Roy. Meteor. Soc.*, **137**, 553–597, doi:[10.1002/qj.828](https://doi.org/10.1002/qj.828).
- Edmon, H. J., B. J. Hoskins, and M. E. McIntyre, 1980: Eliassen–Palm cross sections for the troposphere. *J. Atmos. Sci.*, **37**, 2600–2616, doi:[10.1175/1520-0469\(1980\)037<2600:EPCSFT>2.0.CO;2](https://doi.org/10.1175/1520-0469(1980)037<2600:EPCSFT>2.0.CO;2).
- Eliassen, A., and E. Palm, 1961: On the transfer of energy in stationary mountain waves. *Geophys. Publ.*, **22**, 1–23.
- Hahn, D. G., and S. Manabe, 1975: The role of mountains in the South Asian monsoon circulation. *J. Atmos. Sci.*, **32**, 1515–1541, doi:[10.1175/1520-0469\(1975\)032<1515:TROMIT>2.0.CO;2](https://doi.org/10.1175/1520-0469(1975)032<1515:TROMIT>2.0.CO;2).
- Held, I. M., 1983: Stationary and quasi-stationary eddies in the extratropical atmosphere: Theory. *Large-Scale Dynamical Processes in the Atmosphere*, R. P. Pearce and B. J. Hoskins, Eds., Academic Press, 127–168.
- , and M. Ting, 1990: Orographic versus thermal forcing of stationary waves: The importance of the mean low-level wind. *J. Atmos. Sci.*, **47**, 495–500, doi:[10.1175/1520-0469\(1990\)047<0495:OVTFOS>2.0.CO;2](https://doi.org/10.1175/1520-0469(1990)047<0495:OVTFOS>2.0.CO;2).
- , M. F. Ting, and H. L. Wang, 2002: Northern winter stationary waves: Theory and modeling. *J. Climate*, **15**, 2125–2144, doi:[10.1175/1520-0442\(2002\)015<2125:NWSWTA>2.0.CO;2](https://doi.org/10.1175/1520-0442(2002)015<2125:NWSWTA>2.0.CO;2).
- Hoskins, B. J., and D. J. Karoly, 1981: The steady linear response of a spherical atmosphere to thermal and orographic forcing. *J. Atmos. Sci.*, **38**, 1179–1196, doi:[10.1175/1520-0469\(1981\)038<1179:TSLROA>2.0.CO;2](https://doi.org/10.1175/1520-0469(1981)038<1179:TSLROA>2.0.CO;2).
- , and T. Ambrozzi, 1993: Rossby wave propagation on a realistic longitudinally varying flow. *J. Atmos. Sci.*, **50**, 1661–1671, doi:[10.1175/1520-0469\(1993\)050<1661:RWPOAR>2.0.CO;2](https://doi.org/10.1175/1520-0469(1993)050<1661:RWPOAR>2.0.CO;2).
- Hurrell, J. W., J. J. Hack, D. Shea, J. M. Caron, and J. Rosinski, 2008: A new sea surface temperature and sea ice boundary dataset for the Community Atmosphere Model. *J. Climate*, **21**, 5145–5153, doi:[10.1175/2008JCLI2292.1](https://doi.org/10.1175/2008JCLI2292.1).
- , and Coauthors, 2013: The Community Earth System Model: A framework for collaborative research. *Bull. Amer. Meteor. Soc.*, **94**, 1339–1360, doi:[10.1175/BAMS-D-12-00121.1](https://doi.org/10.1175/BAMS-D-12-00121.1).
- Inatsu, M., H. Mukougawa, and S. P. Xie, 2002: Stationary eddy response to surface boundary forcing: Idealized GCM experiments. *J. Atmos. Sci.*, **59**, 1898–1915, doi:[10.1175/1520-0469\(2002\)059<1898:SERTSB>2.0.CO;2](https://doi.org/10.1175/1520-0469(2002)059<1898:SERTSB>2.0.CO;2).
- Kitoh, A., 2002: Effects of large-scale mountains on surface climate—A coupled ocean–atmosphere general circulation model study. *J. Meteor. Soc. Japan*, **80**, 1165–1181, doi:[10.2151/jmsj.80.1165](https://doi.org/10.2151/jmsj.80.1165).
- , 2004: Effects of mountain uplift on East Asian summer climate investigated by a coupled atmosphere–ocean GCM. *J. Climate*, **17**, 783–802, doi:[10.1175/1520-0442\(2004\)017<0783:EOMUOE>2.0.CO;2](https://doi.org/10.1175/1520-0442(2004)017<0783:EOMUOE>2.0.CO;2).
- Lutsko, N. J., and I. M. Held, 2016: The response of an idealized atmosphere to orographic forcing: Zonal versus meridional propagation. *J. Atmos. Sci.*, **73**, 3701–3718, doi:[10.1175/JAS-D-16-0021.1](https://doi.org/10.1175/JAS-D-16-0021.1).
- Manabe, S., and T. Terpstra, 1974: The effects of mountains on the general circulation of the atmosphere as identified by numerical experiments. *J. Atmos. Sci.*, **31**, 3–42, doi:[10.1175/1520-0469\(1974\)031<0003:TEOMOT>2.0.CO;2](https://doi.org/10.1175/1520-0469(1974)031<0003:TEOMOT>2.0.CO;2).
- Manola, I., F. Selten, H. de Vries, and W. Hazeleger, 2013: “Waveguidability” of idealized jets. *J. Geophys. Res.*, **118**, 10 432–10 440, doi:[10.1002/jgrd.50758](https://doi.org/10.1002/jgrd.50758).
- Maroon, E. A., D. M. W. Frierson, and D. S. Battisti, 2015: The tropical precipitation response to Andes topography and ocean heat fluxes in an aquaplanet model. *J. Climate*, **28**, 381–398, doi:[10.1175/JCLI-D-14-00188.1](https://doi.org/10.1175/JCLI-D-14-00188.1).
- Matsuno, T., 1971: A dynamical model of the stratospheric sudden warming. *J. Atmos. Sci.*, **28**, 1479–1494, doi:[10.1175/1520-0469\(1971\)028<1479:ADMOTS>2.0.CO;2](https://doi.org/10.1175/1520-0469(1971)028<1479:ADMOTS>2.0.CO;2).
- McFarlane, N. A., 1987: The effect of orographically excited gravity wave drag on the general circulation of the lower stratosphere and troposphere. *J. Atmos. Sci.*, **44**, 1775–1800, doi:[10.1175/1520-0469\(1987\)044<1775:TEOOEG>2.0.CO;2](https://doi.org/10.1175/1520-0469(1987)044<1775:TEOOEG>2.0.CO;2).
- Molnar, P., and J. M. Stock, 2009: Slowing of India’s convergence with Eurasia since 20 Ma and its implications for Tibetan mantle dynamics. *Tectonics*, **28**, doi:[10.1029/2008TC002271](https://doi.org/10.1029/2008TC002271).
- , W. R. Boos, and D. S. Battisti, 2010: Orographic controls on climate and paleoclimate of Asia: Thermal and mechanical roles for the Tibetan Plateau. *Annu. Rev. Earth Planet. Sci.*, **38**, 77–102, doi:[10.1146/annurev-earth-040809-152456](https://doi.org/10.1146/annurev-earth-040809-152456).

- Nigam, S., and R. Lindzen, 1989: The sensitivity of stationary waves to variations in the basic state zonal flow. *J. Atmos. Sci.*, **46**, 1746–1768, doi:[10.1175/1520-0469\(1989\)046<1746:TSOSWT>2.0.CO;2](https://doi.org/10.1175/1520-0469(1989)046<1746:TSOSWT>2.0.CO;2).
- , I. M. Held, and S. W. Lyons, 1988: Linear simulation of the stationary eddies in a GCM. Part II: The “mountain” model. *J. Atmos. Sci.*, **45**, 1433–1452, doi:[10.1175/1520-0469\(1988\)045<1433:LSOTSE>2.0.CO;2](https://doi.org/10.1175/1520-0469(1988)045<1433:LSOTSE>2.0.CO;2).
- Plumb, R. A., 1985: On the three-dimensional propagation of stationary waves. *J. Atmos. Sci.*, **42**, 217–229, doi:[10.1175/1520-0469\(1985\)042<0217:OTTDPO>2.0.CO;2](https://doi.org/10.1175/1520-0469(1985)042<0217:OTTDPO>2.0.CO;2).
- Ringler, T. D., and K. H. Cook, 1995: Orographically induced stationary waves—Dependence on latitude. *J. Atmos. Sci.*, **52**, 2548–2560, doi:[10.1175/1520-0469\(1995\)052<2548:OISWDO>2.0.CO;2](https://doi.org/10.1175/1520-0469(1995)052<2548:OISWDO>2.0.CO;2).
- , and —, 1999: Understanding the seasonality of orographically forced stationary waves: Interaction between mechanical and thermal forcing. *J. Atmos. Sci.*, **56**, 1154–1174, doi:[10.1175/1520-0469\(1999\)056<1154:UTSOOF>2.0.CO;2](https://doi.org/10.1175/1520-0469(1999)056<1154:UTSOOF>2.0.CO;2).
- Saulière, J., D. J. Brayshaw, B. Hoskins, and M. Blackburn, 2012: Further investigation of the impact of idealized continents and SST distributions on the Northern Hemisphere storm tracks. *J. Atmos. Sci.*, **69**, 840–856, doi:[10.1175/JAS-D-11-0113.1](https://doi.org/10.1175/JAS-D-11-0113.1).
- Seager, R., D. S. Battisti, J. Yin, N. Gordon, N. Naik, A. C. Clement, and M. A. Cane, 2002: Is the Gulf Stream responsible for Europe’s mild winters? *Quart. J. Roy. Meteor. Soc.*, **128**, 2563–2586, doi:[10.1256/qj.01.128](https://doi.org/10.1256/qj.01.128).
- Sha, Y., Z. Shi, X. Liu, and Z. An, 2015: Distinct impacts of the Mongolian and Tibetan Plateaus on the evolution of the East Asian monsoon. *J. Geophys. Res.*, **120**, 4764–4782, doi:[10.1002/2014JD022880](https://doi.org/10.1002/2014JD022880).
- Shi, Z., X. Liu, Y. Liu, Y. Sha, and T. Xu, 2015: Impact of Mongolian Plateau versus Tibetan Plateau on the westerly jet over North Pacific Ocean. *Climate Dyn.*, **44**, 3067–3076, doi:[10.1007/s00382-014-2217-2](https://doi.org/10.1007/s00382-014-2217-2).
- Smagorinsky, J., 1953: The dynamical influence of large-scale heat sources and sinks on the quasi-stationary mean motions of the atmosphere. *Quart. J. Roy. Meteor. Soc.*, **79**, 342–366, doi:[10.1002/qj.49707934103](https://doi.org/10.1002/qj.49707934103).
- Stevens, B., and Coauthors, 2013: Atmospheric component of the MPI-M Earth System Model: ECHAM6. *J. Adv. Model. Earth Syst.*, **5**, 146–172, doi:[10.1002/jame.20015](https://doi.org/10.1002/jame.20015).
- Takahashi, K., and D. S. Battisti, 2007: Processes controlling the mean tropical Pacific precipitation pattern. Part I: The Andes and the eastern Pacific ITCZ. *J. Climate*, **20**, 3434–3451, doi:[10.1175/JCLI4198.1](https://doi.org/10.1175/JCLI4198.1).
- Takaya, K., and H. Nakamura, 1997: A formulation of a wave-activity flux for stationary Rossby waves on a zonally varying basic flow. *Geophys. Res. Lett.*, **24**, 2985–2988, doi:[10.1029/97GL03094](https://doi.org/10.1029/97GL03094).
- , and —, 2001: A formulation of a phase-independent wave-activity flux for stationary and migratory quasigeostrophic eddies on a zonally varying basic flow. *J. Atmos. Sci.*, **58**, 608–627, doi:[10.1175/1520-0469\(2001\)058<0608:AFOAPI>2.0.CO;2](https://doi.org/10.1175/1520-0469(2001)058<0608:AFOAPI>2.0.CO;2).
- Valdes, P. J., and B. J. Hoskins, 1991: Nonlinear orographically forced planetary waves. *J. Atmos. Sci.*, **48**, 2089–2106, doi:[10.1175/1520-0469\(1991\)048<2089:NOFPW>2.0.CO;2](https://doi.org/10.1175/1520-0469(1991)048<2089:NOFPW>2.0.CO;2).
- Warren, B. A., 1983: Why is no deep-water formed in the North Pacific. *J. Mar. Res.*, **41**, 327–347, doi:[10.1357/002224083788520207](https://doi.org/10.1357/002224083788520207).
- Wilson, C., B. Sinha, and R. G. Williams, 2009: The effect of ocean dynamics and orography on atmospheric storm tracks. *J. Climate*, **22**, 3689–3702, doi:[10.1175/2009JCLI2651.1](https://doi.org/10.1175/2009JCLI2651.1).
- Zappa, G., B. J. Hoskins, and T. G. Shepherd, 2015: Improving climate change detection through optimal seasonal averaging: The case of the North Atlantic jet and European precipitation. *J. Climate*, **28**, 6381–6397, doi:[10.1175/JCLI-D-14-00823.1](https://doi.org/10.1175/JCLI-D-14-00823.1).